Timing and structure of the Younger Dryas event in northern China

Zhi-Bang Ma [a,b,*], Hai Cheng [c,d,e], Ming Tan [a], R. Lawrence Edwards [d], Hong-Chun Li [f], Chen-Feng You [g], Wu-Hui Duan [a], Xu Wang [a], Megan J. Kelly [d]

[a] Key Laboratory of Cenozoic Geology and Environment, Institute of Geology and Geophysics, Chinese Academy of Sciences, Beijing 100029, China
[b] Key Laboratory of Saline Lake Resources and Environment, Ministry of Land and Resources, Beijing 100037, China
[c] Institute of Global Environmental Change, Xi'an Jiaotong University, Xi'an 710049, China
[d] Department of Earth Sciences, University of Minnesota, Minneapolis, MN 55455, USA
[e] State Key Laboratory of Loess and Quaternary Geology, Institute of Earth Environment, Chinese Academy of Sciences, Xi'an 710075, China
[f] Department of Geosciences, National Taiwan University, Taipei 617, Taiwan
[g] Department of Earth Sciences, National Cheng Kung University, Tainan 701, Taiwan

ARTICLE INFO

ABSTRACT

A high-resolution and absolute-dated stalagmite record from Kulishu Cave, Beijing characterizes Asian Monsoon (AM) history in northern China between ca 14 and 10.5 ka BP (thousand yrs before present, present = 1950), including the entire Younger Dryas (YD) event. Using ^{230}Th dates and counting of annual-layers, the shift into the YD began at 12,850 ± 40 yr BP and took ∼340 yrs and the shift out of the YD began at 11,560 ± 40 yr BP and took <38 yrs (best estimate ∼20 yrs), broadly similar to previously reported AM records from central and southeastern China. The more gradual nature of the start of the YD event as observed in the AM records appears to contrast with the more abrupt beginning observed in the Greenland ice records. The total amplitude of the AM YD event is also smaller than the amplitude of the AM Heinrich Stadial 1 event. In addition, the general rising trend of the AM during the Bølling-Allerød period contrasts with the general cooling trend in Greenland temperature during that time. The influence of rising insolation on the AM may explain this observation.

© 2012 Elsevier Ltd. All rights reserved.

1. Introduction

The Younger Dryas (YD) event is a millennial-scale cold period (∼1300 yr duration) between approximately 12,900 and 11,500 yr BP, which punctuated the last glacial termination. During the event, the temperature over central Greenland swung from near-interglacial back to near-glacial conditions, about 15 °C lower than today (Severinghaus et al., 1998). No event in the climate record has received more attention than the YD event (Broecker et al., 2010), yet the geographic extent and the cause of event remain a subject of debate. Recent developments in speleothem studies shed new light on the nature and geographic extent of the event. For example, speleothem records show a period of weakened Asian Monsoon (AM) during the YD event (Wang et al., 2001, 2007; Yuan et al., 2004; Dykoski et al., 2005; Sinha et al., 2005; Shakun et al., 2007; Liu et al., 2008; Yang et al., 2010), a wetter excursion

in Indonesia in the Southern Hemisphere (Griffiths et al., 2009), a generally cold and/or dry climate in France (Genty et al., 2006), Turkey (Fleitmann et al., 2009) and Israel (Bar-Matthews et al., 2003), a cold period in Oregon USA (Vacco et al., 2005), and a wet period in the southwestern U.S. (Asmerom et al., 2010). In addition, speleothem records from South America reveal an intensified South American Summer Monsoon (SASM) during the YD (Cruz et al., 2005, 2009; Wang et al., 2007). Cheng et al. (2009b) also recognized a YD-like event in the AM record superimposed on glacial termination III, which led to the idea that YD-type events may be an integral part of glacial terminations (Broecker et al., 2010). However, it remains unclear how low-mid latitude climates responded to changes in the North Atlantic region, if indeed, the YD event was triggered by events in the North Atlantic. To tackle this issue, it is necessary to obtain additional climate records from the low-mid latitudes, with high-resolution and precise chronology, at least comparable to Greenland ice core records. Speleothem records are one such record as speleothems with the right characteristics can be precisely dated by ^{230}Th methods combined with layer counting. For example, on the basis of both ^{230}Th and annual-layer counting chronology, a recent speleothem record from central China demonstrated that the full

* Corresponding author. Present address: Institute of Geology and Geophysics, Chinese Academy of Sciences, 19 Beitucheng West Road, Chaoyang District, Beijing 100029, China. Tel.: +86 10 82998398; fax: +86 10 62010846.
E-mail address: mzb@mail.iggcas.ac.cn (Z.-B. Ma).

transition of the AM from the late Allerød into the YD lasted about 380 yrs, significantly longer (by ca 130 yrs) than the analogous Greenland temperature shift (Liu et al., 2008).

In this study, we present a new high-resolution, precisely dated speleothem oxygen isotope record from Kulishu Cave, which characterizes the YD event in detail, for the first time in northern China. This record, together with other records from central and southeastern China, provides a structure for AM changes over the YD event with regional spatial coverage. This, in turn, allows us to precisely compare the YD event in AM records with those in Greenland and elsewhere around the world.

2. Cave location and sample

Developed in a Middle Proterozoic dolomite, Kulishu Cave (39°41′ N, 115°39′ E, 610 m a.s.l.) is located on the slope of a hill, which belongs to the Beijing Xishan karst area, approximately 80 km southwest of the city Beijing (Fig. 1). The cave is nearly 60 m deep and has a narrow, steep passage leading from the entrance to a chamber from which stalagmite BW-1 was collected. Although the roof of the cave is about 120 m thick at its thickest, it is only several meters thick at the entrance. The vegetation above the cave is dominated by secondary-growth deciduous broadleaf trees and shrubs. The cave is within the region currently affected by Asian summer monsoon rainfall, but lies close to its northern boundary with the northwestern arid-semiarid zone. The mean annual temperature and precipitation are 12.3 °C and 570 mm in Beijing, respectively (1971–2000 averages, according to Chinese Meteorological Administration data at http://www.cma.gov.cn/) and the summer precipitation accounts for 74% of the annual precipitation. The cave temperature varies between 16 °C in July and 6 °C in January, due to the relatively large open entrance at present. Field observations show that the drip rate of cave water responds to seasonal cycle of precipitation sensitively without significant lag. Like the nearby Shihua Cave (Fig. 1), the strong seasonal variations in temperature, precipitation, and vegetation favor the formation of annual-layers during speleothem growth (Tan et al., 2003). The regional pattern of seasonal changes in modern precipitation $\delta^{18}O$ is similar to those described in Cheng et al., 2006 and 2009b (and references therein), with low precipitation $\delta^{18}O$ values tied with Asian summer monsoon precipitation. We collected a stalagmite, BW-1, from Kulishu Cave about 40 m from the entrance in October 1999. The sample is 19.5 cm high and 10 cm wide.

3. Methods

We cut the stalagmite in half along the growth axis (Fig. 2). The polished stalagmite appeared pristine without any visible post-depositional recrystallization. A total of 235 sub-samples for oxygen isotope analysis were collected in two ways: 1) drilled using a 0.5 mm carbide dental burr at an average interval of 1 mm; and 2) shaved using a knife at an average resolution of approximately 12 sub-samples per mm. An additional 20 samples were drilled along stratigraphic horizons for the Hendy test (Hendy, 1971). Each sub-sample weighed about 150 μg. Stable isotope analyses were
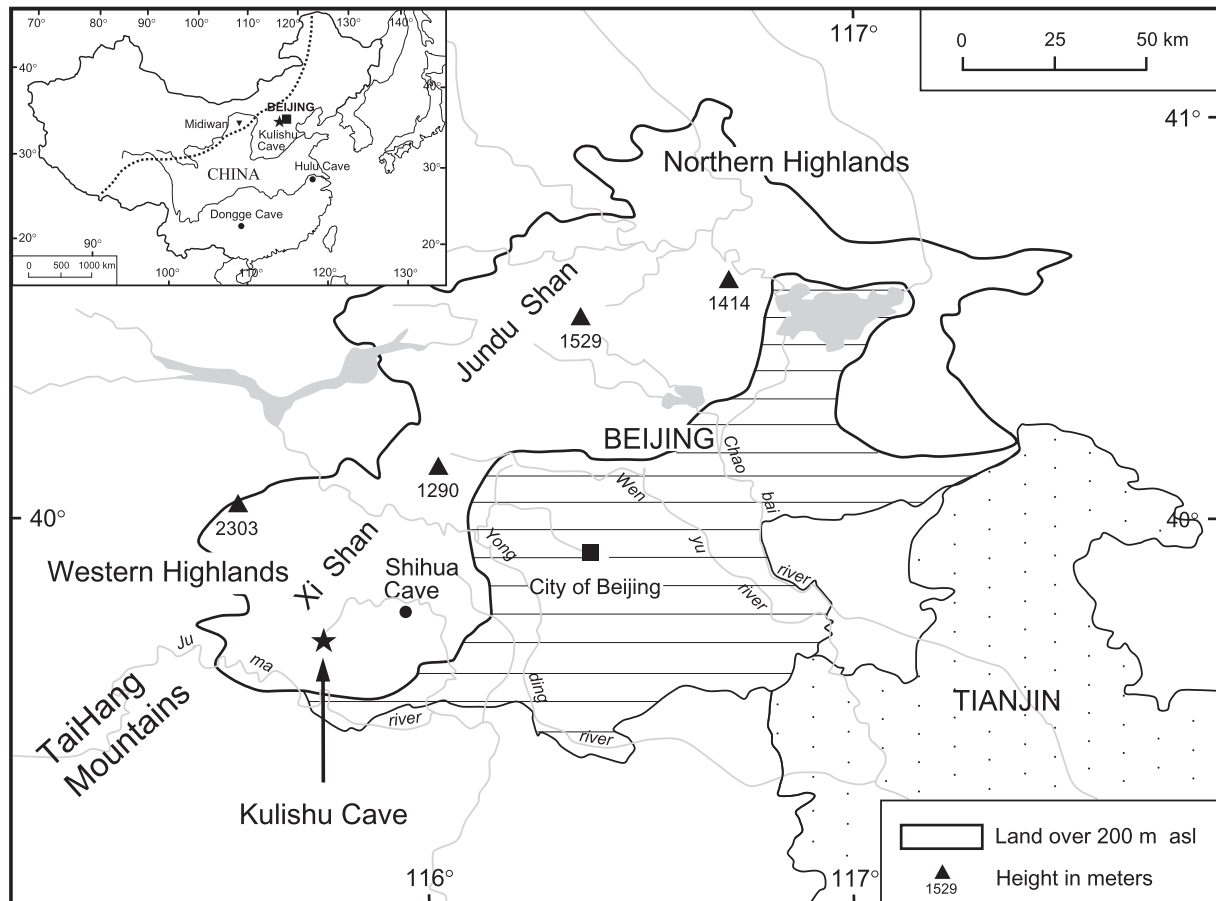

Fig. 1. Location of Kulishu Cave (39°41′ N, 115°39′ E) near Beijing (compiled from Ku and Li, 1998). Inset: locations of Kulishu Cave and Midiwan site in northern China, and Hulu Cave and Dongge Cave in southeastern China. The dashed lines represent the approximate northwestern fringe of the Asian summer monsoon at present.
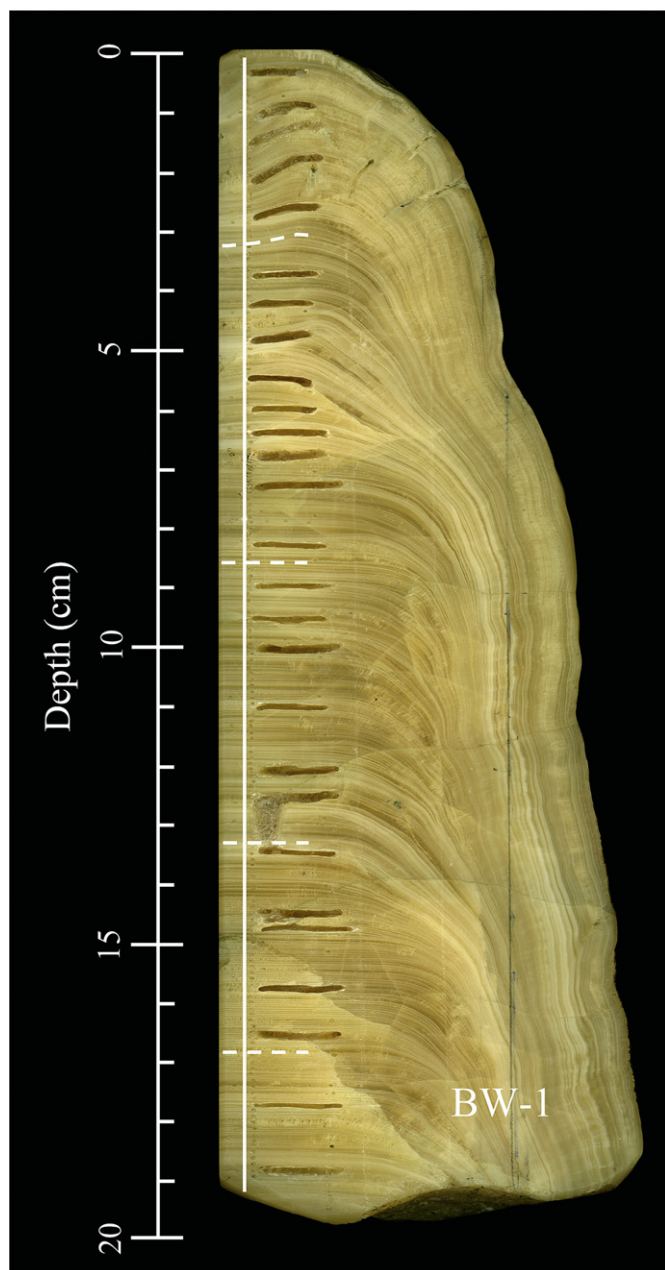
Fig. 2. Image of stalagmite BW-1. Holes can be seen where samples were drilled for [230]Th dating. The white vertical line shows the track of sub-samples for stable isotope analysis, and dashed lines indicate the positions of samples for Hendy Test.

Fig. 3. (a) [230]Th age model for the stalagmite BW-1. All ages are in stratigraphic order within dating errors (2σ). (b) BW-1 growth rate versus time.

performed in the Environmental Isotope Laboratory, Institute of Geology and Geophysics, Chinese Academy of Sciences, using a MAT-253 mass spectrometer connected to a Gas Bench-II (Thermo-Finnigan) device for reaction of powdered carbonate with 100% H_3PO_4 at 72° C. A standard (NBS-19) was analyzed every six samples. Based on the reproducibility of the standard runs, we estimated the one-sigma error to be ±0.1‰. All oxygen isotope values are reported in parts per mil (‰) relative to Vienna Pee Dee Belemnite (VPDB) ($\delta^{18}O$). Based on [230]Th dating results (Fig. 3 and Table 1), 235 stable isotope analyses (Table 2) yielded temporal resolutions ranging between 1 and 29 yrs, averaging ~14 yrs.

Powdered sub-samples (approximately 200 mg) from BW-1 were drilled along growth bands using a 0.9 mm carbide dental burr for [230]Th dating. We obtained 26 [230]Th dates at the Minnesota
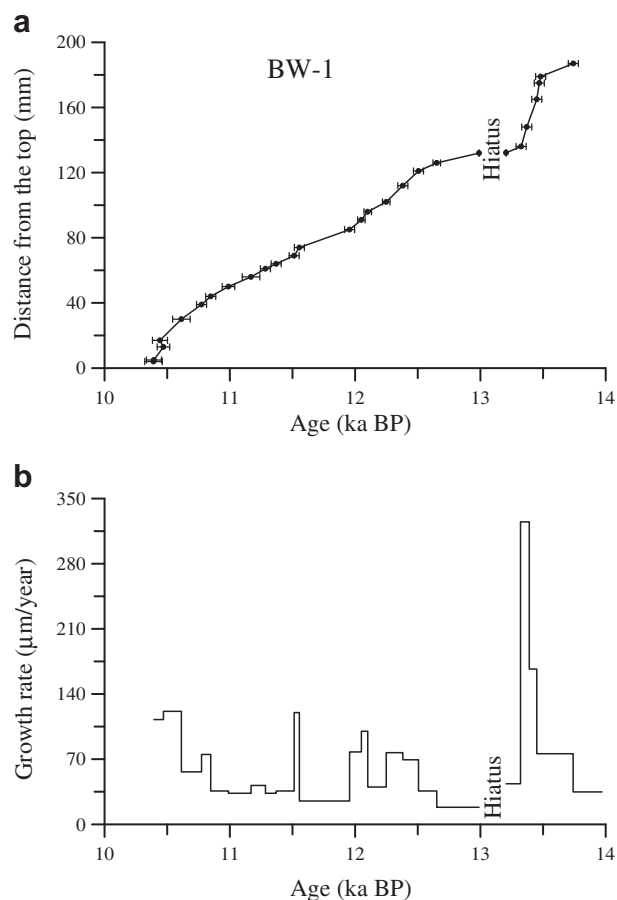
Isotope Laboratory, Department of Earth Sciences, University of Minnesota using a multi-collector inductively-coupled plasma mass spectrometer (a Thermo-Scientific Neptune). Chemical separation procedures are similar to those described in Edwards et al. (1987), and details on instrumental approaches have been described by Cheng et al. (2000), Shen et al. (2002), and Cheng et al. (2009a, 2009b). A [230]Th/[232]Th atomic ratio of $4.4 \pm 2.2 \times 10^{-6}$ was used to correct for the initial [230]Th. Linear interpolation was used to establish the age model.

Thin sections were prepared to investigate the features and thicknesses of micro-bands under an Olympus stereo microscope with a Nikon camera connected to a computer. One annual-layer is composed of a pair of light and dark colored bands, but contrary to the transmitted light images described by Tan et al. (2003, 2006). To reduce statistical errors during layer counting, we counted bands multiple times with different people. Uncertainties are within a range of 2%–3%.

4. Results

4.1. Chronology

Dating results are presented in Table 1. All ages are in stratigraphic order within dating errors. The age model is shown in Fig. 3a. We count a total of 1573 annual-layers between 4 and 85 mm from the top of the sample, corresponding to the time period between the early Holocene and the middle of the YD event, consistent within errors with the [230]Th dating results. However, it is difficult to count layers between 86 and 195 mm

Table 1
[230]Th dating results of stalagmite BW-1 from Kulishu Cave. The bold values represent that the error is a 2σ error.

Sample number	U (ppb)	Th (ppt)	[230]Th/[232]Th (atomic × 10⁻⁶)	δ^{234}U[a] (measured)	[230]Th/[238]U (activity)	[230]Th age (yr BP) (uncorrected)	[230]Th age (yr) (corrected)	δ[234]U_Initial[b] (corrected)
BW-1-1	261.3 ± 0.3	887 ± 18	620 ± 13	381.7 ± 2.0	0.1276 ± 0.0005	10,462 ± 43	**10,390 ± 70**	393 ± 2
BW-1-T	215.4 ± 0.2	699 ± 14	649 ± 13	382.0 ± 1.8	0.1276 ± 0.0004	10,461 ± 37	**10,390 ± 60**	393 ± 2
BW-1-2	276.2 ± 0.2	663 ± 13	884 ± 18	384.9 ± 1.7	0.1286 ± 0.0004	10,519 ± 35	**10,470 ± 50**	397 ± 2
BW-1-3	333.1 ± 0.4	1091 ± 22	643 ± 13	376.9 ± 1.7	0.1277 ± 0.0004	10,510 ± 60	**10,440 ± 60**	388 ± 2
BW-1-3a	300.6 ± 0.4	1185 ± 24	545 ± 11	381.1 ± 2.1	0.1303 ± 0.0004	10,695 ± 39	**10,610 ± 70**	393 ± 2
BW-1-3b	367.9 ± 0.4	674 ± 14	1178 ± 24	372.5 ± 1.8	0.1308 ± 0.0003	10,813 ± 34	**10,770 ± 40**	384 ± 2
BW-1-3c	413.6 ± 0.6	737 ± 15	1220 ± 25	374.4 ± 1.8	0.1318 ± 0.0003	10,884 ± 33	**10,850 ± 40**	386 ± 2
BW-1-4	361.1 ± 0.3	779 ± 16	1016 ± 21	369.0 ± 1.6	0.1330 ± 0.0003	11,034 ± 33	**10,990 ± 50**	381 ± 2
BW-1-4a	447 ± 1	1983 ± 40	504 ± 10	366.8 ± 1.7	0.1354 ± 0.0003	11,263 ± 32	**11,170 ± 70**	379 ± 2
BW-1-4b	504 ± 1	766 ± 15	1481 ± 30	371.0 ± 1.8	0.1364 ± 0.0003	11,316 ± 32	**11,280 ± 40**	383 ± 2
BW-1-4c	486 ± 1	782 ± 16	1406 ± 28	367.5 ± 1.8	0.1371 ± 0.0003	11,404 ± 30	**11,370 ± 40**	380 ± 2
BW-1-5	597 ± 1	868 ± 17	1583 ± 32	376.8 ± 2.0	0.1396 ± 0.0003	11,543 ± 29	**11,510 ± 40**	389 ± 2
BW-1-6	660 ± 1	1244 ± 25	1240 ± 25	393.6 ± 2.0	0.1419 ± 0.0002	11,593 ± 27	**11,560 ± 40**	407 ± 2
BW-1-6a	697 ± 1	956 ± 19	1757 ± 35	391.8 ± 1.7	0.1462 ± 0.0003	11,983 ± 30	**11,960 ± 40**	405 ± 2
BW-1-6b	834 ± 1	697 ± 14	2904 ± 59	392.2 ± 1.9	0.1472 ± 0.0003	12,067 ± 31	**12,050 ± 30**	406 ± 2
BW-1-6c	730 ± 1	397 ± 8	4441 ± 91	379.4 ± 1.7	0.1464 ± 0.0003	12,113 ± 29	**12,100 ± 30**	393 ± 2
BW-1-7	740 ± 1	228 ± 5	7940 ± 160	385.9 ± 1.7	0.1487 ± 0.0003	12,253 ± 29	**12,250 ± 30**	400 ± 2
BW-1-7a	765 ± 1	842 ± 17	2241 ± 45	377.2 ± 1.8	0.1495 ± 0.0004	12,403 ± 37	**12,380 ± 40**	391 ± 2
BW-1-8	783 ± 1	1019 ± 20	1912 ± 38	376.8 ± 1.9	0.1509 ± 0.0003	12,533 ± 30	**12,510 ± 30**	390 ± 2
BW-1-9	749 ± 1	473 ± 10	3966 ± 80	373.8 ± 1.8	0.1520 ± 0.0002	12,664 ± 28	**12,650 ± 30**	387 ± 2
BW-1-9a	1030 ± 1	1868 ± 37	1415 ± 28	337.9 ± 1.8	0.1557 ± 0.0003	13,363 ± 33	**13,320 ± 40**	351 ± 2
BW-1-10	1355 ± 2	2056 ± 41	1697 ± 34	338.1 ± 1.8	0.1561 ± 0.0003	13,400 ± 33	**13,360 ± 40**	351 ± 2
BW-1-10a	1576 ± 2	1481 ± 30	2761 ± 56	342.5 ± 1.7	0.1574 ± 0.0004	13,467 ± 37	**13,450 ± 40**	356 ± 2
BW-1-B	1159 ± 2	1116 ± 22	2693 ± 54	339.7 ± 1.6	0.1573 ± 0.0003	13,494 ± 36	**13,470 ± 40**	353 ± 2
BW-1-11a	1512 ± 2	1536 ± 31	2545 ± 51	334.5 ± 1.7	0.1568 ± 0.0003	13,503 ± 33	**13,480 ± 40**	348 ± 2
BW-1-12	2122 ± 4	653 ± 13	8598 ± 173	340.6 ± 1.8	0.1602 ± 0.0003	13,749 ± 35	**13,740 ± 40**	354 ± 2

Decay Constants are described in Cheng et al., 2009a and 2009b.
Corrected [230]Th ages assume the initial [230]Th/[232]Th atomic ratio of 4.4 ± 2.2 × 10⁻⁶. Those are the values for a material at secular equilibrium, with the bulk earth [232]Th/[238]U value of 3.8. The errors are arbitrarily assumed to be 50%.

[a] $\delta^{234}U = ([^{234}U/^{238}U]_{activity} - 1) \times 1000$.
[b] $\delta^{234}U_{initial}$ was calculated based on [230]Th age (T), i.e., $\delta^{234}U_{initial} = \delta^{234}U_{measured} \times e^{\lambda_{234} \times T}$.

where annual-layers are not clear enough to be counted definitively. Growth rates of the sample vary from 18 to 325 μm/yr with an average of 76 μm/yr (Fig. 3b). The growth rate is relatively low during the YD interval (~59 μm/yr) and, overall, higher growth rates correspond to low δ^{18}O phases. This implies an inverse correlation between the precipitation δ^{18}O and the amount of Asian summer monsoon rainfall.

4.2. δ^{18}O proxy

Following Hendy (1971), 20 sub-samples from four growth bands were analyzed (Fig. 4a and b). Slopes of linear regressions of δ^{18}O versus δ^{13}C values are 0.16, 0.02, 0.07 and 0.10, respectively (Fig. 4b), with no significant correlation between δ^{18}O and distance from the growth axis (Fig. 4b), suggesting that kinetic fractionation had little effect. Hence, variations in δ^{18}O of stalagmite calcite (δ[18]O_c) mainly reflect dripwater δ^{18}O (δ[18]O_p) and cave temperature (Hendy, 1971). Of note is the large range of δ[18]O_c fluctuations on centennial and decadal timescales (as large as 3.5‰). This suggests the primary control on calcite δ[18]O_c is the δ[18]O_p of monsoonal precipitation, rather than temperature, as explained by numerous investigations (Wang et al., 2001; Dykoski et al., 2005; Kelly et al., 2006; Liu et al., 2008; Cheng et al., 2009b and others).

Dripwater in many caves originates from meteoric precipitation. Provided δ[18]O_p did not shift before calcite deposition, changes in δ[18]O_c would mainly reflect changes in δ[18]O_p, which, in turn, is a function of the moisture sources and the evolution of moisture in air masses as it moves from the source to the cave site (Dansgaard, 1964; Li et al., 2007; Lachniet, 2009). In the case of Kulishu Cave, precipitation is dominated by the summer monsoon (mainly during July–August), when the land-sea temperature gradient reaches a maximum and the intertropical convergence zone (ITCZ) shifts far to the north. In contrast, cold–dry winds prevail during the winter

under the influence of the Siberian-High, resulting in little precipitation in the area. As expected, the Kulishu δ^{18}O record is similar to the Hulu-Dongge-Yamen-Qingtian-Sanbao records (Wang et al., 2001, 2008; Yuan et al., 2004; Dykoski et al., 2005; Liu et al., 2008; Yang et al., 2010) (Figs. 5 and 7). In comparison to Hulu and Dongge records from southeastern China, however, δ^{18}O values of the Kulishu record are lower by ~1.0‰, illustrating a general "continental effect" that is broadly consistent with the observation that modern δ^{18}O values of cave dripwater and surface water become progressively lower northward along the moisture transport trajectory (Li et al., 2007).

It is now evident that cave δ^{18}O variability in the AM region is consistent at least during the YD event, despite local precipitation differences between northern and southern China. This supports earlier interpretations of the δ^{18}O in Chinese cave deposits: changes in the proportion of summer monsoon rainfall in annual totals play a significant role in governing the pattern of precipitation δ^{18}O changes (Wang et al., 2008; Cheng et al., 2009b). Accordingly, more negative/positive δ^{18}O excursions in the Kulishu Cave speleothems mostly indicate higher/lower proportions of summer monsoon rainfall (low δ^{18}O rainfall) in annual totals (e.g., Cheng et al., 2009b).

Other paleoclimate records from the area also point to a general cold–dry period during the YD event. An organic δ^{13}C record from the Midiwan peat profile, near the Chinese loess-desert transitional belt, revealed an interruption of the deglacial trend with cold–dry to cool–humid to cold–dry fluctuations on centennial scales during the YD (Zhou et al., 2001). These observations are consistent with an increase in herbaceous pollen in northern China (Sun and Chen, 1991; Yi and Saito, 2004), and drops in lake-level during the event in both the Beijing area (Wei et al., 1997) and adjacent Inner Mongolia (Wang et al., 1994; Peng et al., 2005). These records support the above-mentioned AM δ^{18}O interpretation based on speleothem records.

Table 2
δ^{18}O and δ^{13}C data for stalagmite BW-1 from Kulishu Cave. Depths are relative to the top (youngest surface) of stalagmite and are measured along the growth axis. Ages are established by [230]Th dates.

Depths (mm)	Age (yrs/1950)	±2σ errors	δ^{18}O (‰, VPDB)	δ^{13}C (‰, VPDB)
1	10,378		−9.39	−9.48
2	10,382		−10.23	−8.91
3	10,386		−9.13	−9.11
4	**10,390**	**70**	−9.25	−9.59
5	**10,390**	**60**	−9.47	−9.59
6	10,394		−10.25	−9.93
7	10,398		−9.79	−10.18
8	10,403		−9.91	−10.59
9	10,407		−9.90	−10.76
10	10,411		−9.66	−11.01
11	10,415		−9.82	−10.82
12	10,419		−9.18	−9.44
13	**10,470**	**50**	−9.43	−10.05
14	10,428		−8.93	−9.32
15	10,432		−8.92	−9.76
16	10,436		−9.27	−9.77
17	**10,440**	**60**	−9.49	−10.37
18	10,453		−9.64	−10.31
19	10,466		−10.34	−9.63
20	10,479		−9.74	−10.52
21	10,492		−10.11	−9.62
22	10,505		−10.33	−10.08
23	10,518		−10.23	−10.86
24	10,532		−9.17	−10.25
25	10,545		−10.26	−9.98
26	10,558		−9.75	−10.06
27	10,571		−9.23	−10.66
28	10,584		−9.95	−11.01
29	10,597		−9.17	−10.60
30	**10,610**	**70**	−9.79	−10.98
31	10,628		−9.65	−10.30
32	10,646		−9.38	−9.44
33	10,663		−8.83	−9.77
34	10,681		−8.35	−10.24
35	10,699		−8.93	−9.31
36	10,717		−8.77	−9.38
37	10,734		−8.49	−9.16
38	10,752		−8.31	−9.35
39	**10,770**	**40**	−8.22	−9.70
40	10,783		−8.42	−9.54
41	10,797		−8.88	−9.44
42	10,810		−9.26	−9.07
43	10,823		−8.92	−9.63
44	10,837		−7.99	−9.49
45	**10,850**	**40**	−8.80	−9.61
46	10,878		−9.37	−10.20
47	10,906		−8.67	−10.05
48	10,934		−8.17	−9.31
49	10,962		−7.92	−9.81
50	**10,990**	**50**	−8.04	−10.05
51	11,020		−8.70	−9.58
52	11,050		−8.51	−10.18
53	11,080		−9.01	−10.41
54	11,110		−8.65	−10.63
55	11,140		−9.10	−10.45
56	**11,170**	**70**	−8.94	−10.06
57	11,192		−8.96	−10.15
58	11,214		−7.79	−10.13
59	11,236		−8.33	−9.90
60	11,258		−8.50	−9.77
61	**11,280**	**40**	−8.78	−9.83
62	11,310		−9.28	−10.27
63	11,340		−9.65	−9.69
64	**11,370**	**40**	−8.93	−10.55
65	11,398		−8.57	−10.42
66	11,426		−8.99	−9.47
67	11,454		−8.22	−10.27
68	11,482		−8.94	−10.11
69	**11,510**	**40**	−8.98	−9.34
70	11,520		−8.61	−9.45
71	11,530		−7.61	−9.45
72	11,540		−7.09	−9.56
73	11,550		−6.84	−9.02

Table 2 (*continued*)

Depths (mm)	Age (yrs/1950)	±2σ errors	δ^{18}O (‰, VPDB)	δ^{13}C (‰, VPDB)
74	**11,560**	**40**	−6.75	−8.75
75	11,584		−7.11	−7.37
76	11,607		−7.43	−9.38
77	11,631		−7.31	−9.08
77.5	11,654		−7.17	−7.93
78	11,678		−7.34	−8.32
78.5	11,701		−7.55	−8.27
79	11,725		−7.27	−8.33
79.5	11,748		−7.43	−8.25
80	11,772		−7.58	−8.49
80.5	11,795		−7.54	−8.03
81	11,819		−7.16	−7.61
81.5	11,842		−7.51	−7.46
82	11,866		−7.39	−7.19
82.5	11,889		−7.70	−8.14
83	11,913		−8.45	−8.77
83.5	11,936		−8.68	−8.91
84	**11,960**	**40**	−8.75	−9.07
85	11,973		−7.71	−9.17
86	11,986		−8.13	−9.58
87	11,999		−7.60	−8.88
88	12,011		−7.44	−9.11
89	12,024		−7.48	−8.92
90	12,037		−7.73	−8.42
91	**12,050**	**30**	−7.21	−8.45
92	12,060		−7.43	−8.60
93	12,070		−7.65	−8.55
94	12,080		−7.93	−9.01
95	12,090		−7.67	−8.81
96	**12,100**	**30**	−8.56	−8.56
97	12,125		−8.36	−8.54
98	12,150		−8.05	−8.79
99	12,175		−7.01	−7.94
100	12,200		−6.93	−7.60
101	12,225		−7.11	−7.19
102	**12,250**	**30**	−7.00	−8.61
103	12,263		−7.36	−8.81
104	12,276		−7.73	−9.34
105	12,289		−7.76	−9.71
106	12,302		−7.61	−9.15
107	12,315		−7.55	−9.56
108	12,328		−7.80	−10.11
109	12,341		−7.91	−9.66
110	12,354		−8.35	−10.18
111	12,367		−8.26	−9.64
112	**12,380**	**40**	−7.76	−9.21
113	12,394		−7.74	−9.49
114	12,409		−8.44	−9.85
115	12,423		−8.48	−9.89
116	12,438		−7.55	−9.30
117	12,452		−7.51	−8.91
118	12,467		−8.22	−9.51
119	12,481		−7.72	−9.19
120	12,496		−7.98	−9.26
121	**12,510**	**40**	−7.24	−8.09
122	12,538		−7.48	−8.37
123	12,566		−8.03	−8.90
124	12,594		−7.61	−8.09
125	12,622		−8.20	−8.24
126	**12,650**	**30**	−8.36	−9.43
126.1	12,664		−8.46	−9.18
126.3	12,677		−8.60	−9.05
126.6	12,691		−8.20	−9.24
126.8	12,704		−8.92	−9.07
127	12,718		−8.55	−10.08
127.3	12,731		−8.81	−9.72
127.6	12,745		−8.99	−10.11
127.8	12,758		−8.70	−10.06
128	12,772		−9.13	−10.03
128.3	12,786		−8.88	−9.44
128.6	12,799		−8.80	−9.58
128.8	12,813		−9.23	−10.43
129	12,826		−9.42	−10.44
129.3	12,840		−9.05	−10.17
129.6	12,853		−9.17	−9.80

Table 2 (continued)

Depths (mm)	Age (yrs/1950)	±2σ errors	δ^{18}O (‰, VPDB)	δ^{13}C (‰, VPDB)
129.8	12,867		−9.50	−9.16
130	12,881		−9.06	−9.28
130.3	12,894		−9.44	−8.96
130.5	12,908		−9.29	−8.63
130.7	12,921		−8.97	−8.88
130.9	12,935		−8.97	−9.14
131	12,948		−9.44	−9.28
131.3	12,962		−9.02	−9.84
131.6	12,975		−8.93	−9.14
131.8	12,989		−8.84	−9.57
Hiatus				
132	**13,205**		−9.37	−9.27
132.3	13,212		−8.97	−9.31
132.6	13,219		−8.68	−9.18
132.8	13,227		−8.52	−9.72
133	13,234		−8.39	−9.06
133.3	13,241		−8.55	−9.96
133.6	13,248		−8.56	−9.85
133.8	13,255		−8.73	−9.45
134	13,263		−9.09	−9.21
134.3	13,270		−9.67	−8.80
134.6	13,277		−8.59	−10.08
134.8	13,284		−8.60	−9.72
135	13,291		−9.55	−10.11
135.3	13,298		−8.91	−10.06
135.6	13,306		−8.70	−10.03
135.8	13,313		−8.61	−9.44
136	**13,320**	40	−9.49	−9.58
137	13,323		−9.37	−9.76
138	13,326		−9.07	−10.36
139	13,329		−8.57	−9.73
140	13,332		−8.77	−9.87
141	13,335		−8.85	−10.04
142	13,338		−8.77	−9.95
143	13,341		−8.96	−10.28
144	13,344		−9.55	−10.40
145	13,347		−9.56	−9.94
146	13,350		−9.16	−10.38
147	13,354		−9.44	−10.68
148	13,357		−9.77	−10.64
149	**13,360**	40	−9.04	−10.59
150	13,366		−9.31	−10.43
151	13,371		−9.47	−10.24
152	13,377		−9.33	−10.35
153	13,383		−9.18	−10.67
154	13,388		−9.44	−10.08
155	13,394		−9.37	−10.44
156	13,399		−9.10	−10.29
157	13,405		−9.20	−10.35
158	13,411		−9.07	−10.61
159	13,416		−9.29	−10.13
160	13,422		−9.24	−10.90
161	13,428		−9.30	−10.34
162	13,433		−9.39	−10.55
163	13,439		−9.97	−10.67
164	13,444		−9.82	−10.74
165	**13,450**	40	−10.04	−10.17
166	13,452		−9.60	−10.57
167	13,454		−9.30	−9.77
168	13,456		−9.96	−9.14
169	13,458		−9.58	−9.32
170	13,460		−9.40	−9.77
171	13,462		−9.48	−10.09
172	13,464		−9.08	−9.56
173	13,466		−9.01	−10.13
174	13,468		−9.15	−10.29
175	**13,470**	40	−8.59	−10.17
176	13,473		−8.57	−10.28
177	13,477		−9.16	−9.82
178	**13,480**	40	−9.58	−10.24
179	13,509		−8.90	−9.93
180	13,538		−9.60	−10.63
181	13,567		−8.93	−10.15
182	13,596		−8.54	−9.87
183	13,624		−9.23	−10.41
184	13,653		−9.36	−9.55

Table 2 (continued)

Depths (mm)	Age (yrs/1950)	±2σ errors	δ^{18}O (‰, VPDB)	δ^{13}C (‰, VPDB)
185	13,682		−9.80	−10.09
186	13,711		−9.32	−9.77
187	**13,740**	40	−8.52	−9.66
188	13,769		−8.63	−9.39
189	13,798		−8.61	−9.29
190	13,827		−9.30	−9.41
191	13,856		−8.57	−9.58
192	13,884		−9.12	−9.72
193	13,913		−8.99	−9.91
194	13,942		−9.23	−9.57
195	13,971		−8.98	−9.25

5. Discussion

5.1. Kulishu δ^{18}O record and comparison with other records

The Kulishu record covers a time period from 13,970 to 10,390 yr BP. The δ^{18}O values across this period vary from −6.8 to −10.3‰, averaging −8.7‰ (Table 2). Between 13,970 and 12,850 yr BP, there is a hiatus at ~132 mm depth, noticeable because of a color change. Two dates from below and above the hiatus are 13,320 ± 40 yr BP at 136 mm and 12,650 ± 30 yr BP at 126 mm, giving an approximate age difference of 670 yrs. Layer counting, however, yields only 460 yrs within the same interval, suggesting the hiatus lasted 210 yrs. On the basis of ^{230}Th dates and layer counting, this hiatus can be correlated to the intra-Allerød cold period (IACP), identified previously in the Qingtian record (Fig. 5) as a weak monsoon event between the Early and Late Allerød periods (Liu et al., 2008), and also evident in the Dongge Cave (Dykoski et al., 2005) and Hulu Cave (Wang et al., 2001) records. The transition from the Late Allerød into the YD in the Kulishu record took approximately 340 yrs based on annual-layer counting, similar to the Qingtian record from central China (Liu et al., 2008) (Figs. 5 and 7). The δ^{18}O values representative of the YD period, between 12,850 and 11,560 yr BP, are generally heavier, averaging −7.9‰. The δ^{18}O reached the heaviest values (−6.8‰) of the entire record at 11,560 ± 40 yr BP, followed closely by the end of the YD which is marked by an abrupt jump (more than 2‰) to much lighter values (approximately −9.0‰) at 11,510 ± 40 yr BP. The post-YD decrease in δ^{18}O in the Kulishu record appears to have occurred in two jumps. The first jump is the shift out of the YD and the second takes place at about 10,900 BP. Between the first and second jump, the average δ^{18}O is −8.7‰. After the second jump, the average δ^{18}O is −9.4‰, from 10,900 to the end of the record (10,390 yr BP). Also of note is the abrupt high δ^{18}O excursion centered at about 11,300 yr BP, which likely correlates to the Preboreal Oscillation, which has previously been identified in AM records further to the south (Cai et al., 2008) and is a well known and widespread event, which is clear in records of Greenland ice (e.g., Alley et al., 1993; Rasmussen et al., 2006). The overall pattern of δ^{18}O variation during the early Holocene is broadly similar to those revealed by Greenland ice cores and the Hulu Cave record from southeastern China. The Kulishu record is also characterized by centennial scale events during the YD, centered at 12,410, 12,100 and 11,930 yr BP (A1′, A2′ and A3′ in Fig. 9). These are coincident within error with the similar events in the NGRIP record centered at 12,490, 12,160 and 12,010 yr BP, respectively (A1, A2 and A3 in Fig. 9).

The transition into the YD began at 12,850 ± 40 yr BP in the Kulishu record, consistent with the 12,820 ± 60 yr BP age reported for the Hulu record (Wang et al., 2001), 12,800 ± 140 yr BP in the Dongge record (Dykoski et al., 2005), 12,870 ± 140 yr BP in NGRIP

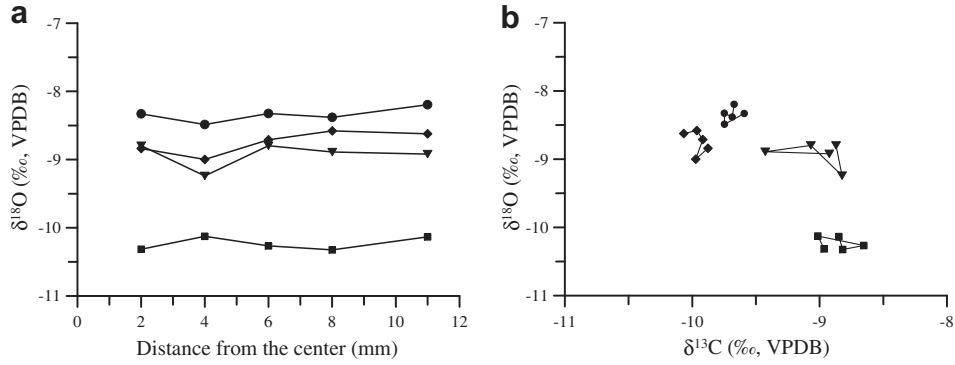**Fig. 4.** The "Hendy Test" (Hendy, 1971): (a) $\delta^{18}O$ variations along four growth layers. (b) $\delta^{18}O-\delta^{13}C$ correlations along four layers. Different layers are denoted respectively by diamonds (33 mm from the top), circles (86 mm), triangles (132 mm) and squares (168 mm). Along each layer, $\delta^{18}O$ values are essentially the same and $\delta^{18}O$ and $\delta^{13}C$ show no statistically significant correlations, suggesting that the stalagmite most likely grew in isotopic equilibrium (Hendy, 1971).
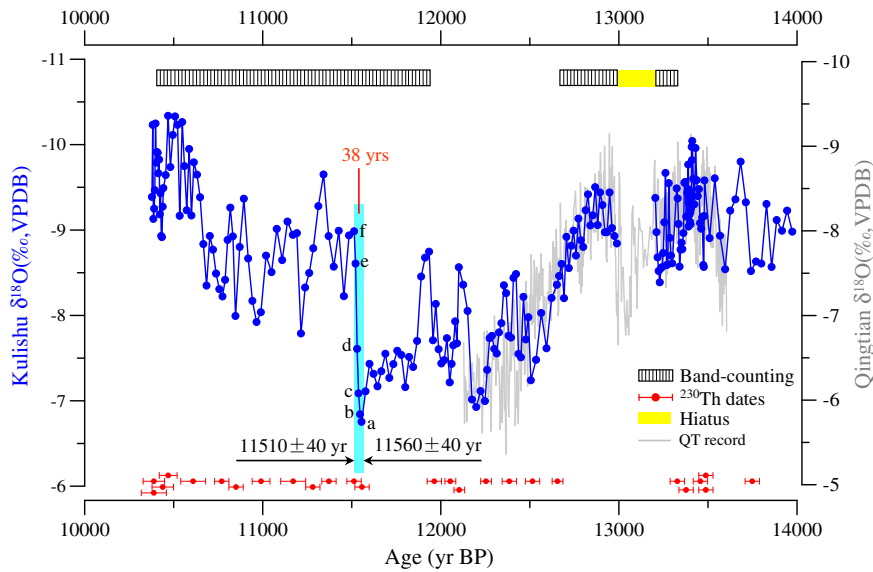
Fig. 5. Kulishu (blue) and Qingtian (gray, Liu et al., 2008) $\delta^{18}O$ records. The ^{230}Th dating errors (2σ) are indicated at the bottom. The annual-layer counting and hiatus intervals are marked by black and yellow bars at the top. The vertical light-blue bar shows the abrupt end of the YD, which has duration of <38 yrs as determined by the annual-layer counting (see Fig. 6 for the image). (For interpretation of the references to color in this figure legend, the reader is referred to the web version of this article.)
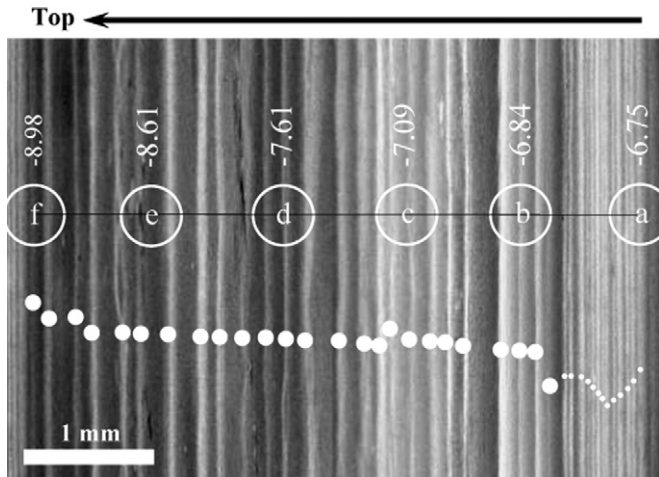
Fig. 6. Reflected light image of the stalagmite BW-1 between 69 and 74 mm. This interval includes the 38 annual bands covering the full $\delta^{18}O$ shift at the end of the YD event. Solid white dots denote the light-color band in each annual-layer. Open circles (a–f) are sub-sample positions for $\delta^{18}O$ analysis (see Fig. 5), and the $\delta^{18}O$ values are marked above circles (in ‰, VPDB). Most of the shift in $\delta^{18}O$ values occurs between points b and e, containing ~20 annual-layers.

(Rasmussen et al., 2006) and 12,890 ± 260 yr BP in GISP2 (Meese et al., 1997). A striking feature of the Kulishu record is its asymmetrical YD structure, with a gradual transition into the event (~340 yrs) and an abrupt ending (<38 yrs or best estimate of 20 yrs) based on annual-layer counting results (Figs. 5 and 6). It is now evident that this distinct asymmetrical YD feature is regional in extent, characteristic of records from AM locations separated by thousands of kilometers (Hulu, Qingtian, Dongge, Timta, Moomi and Kulishu Caves) (Fig. 8). The best age control of the AM YD structure comes from layer counting across speleothem $\delta^{18}O$ shifts. The full transition into the YD took 380 yrs according to the layer-counted Qingtian record (Liu et al., 2008), and the transition out of the YD took about 20 yrs according to the layer-counted Kulishu record (Figs. 5 and 6). While the detailed, asymmetric AM YD structure is consistent across China, records from Greenland (Alley et al., 1993; Rasmussen et al., 2006) and around the North Atlantic basin (i.e. Hughen et al., 1996; von Grafenstein et al., 1999; Haug et al., 2001; Genty et al., 2006), along with recently reported speleothem $\delta^{18}O$ records from Turkey (Fleitmann et al., 2009) and the southwestern United States (Asmerom et al., 2010) may have experienced a more abrupt transition into the YD (Figs. 7 and 8).
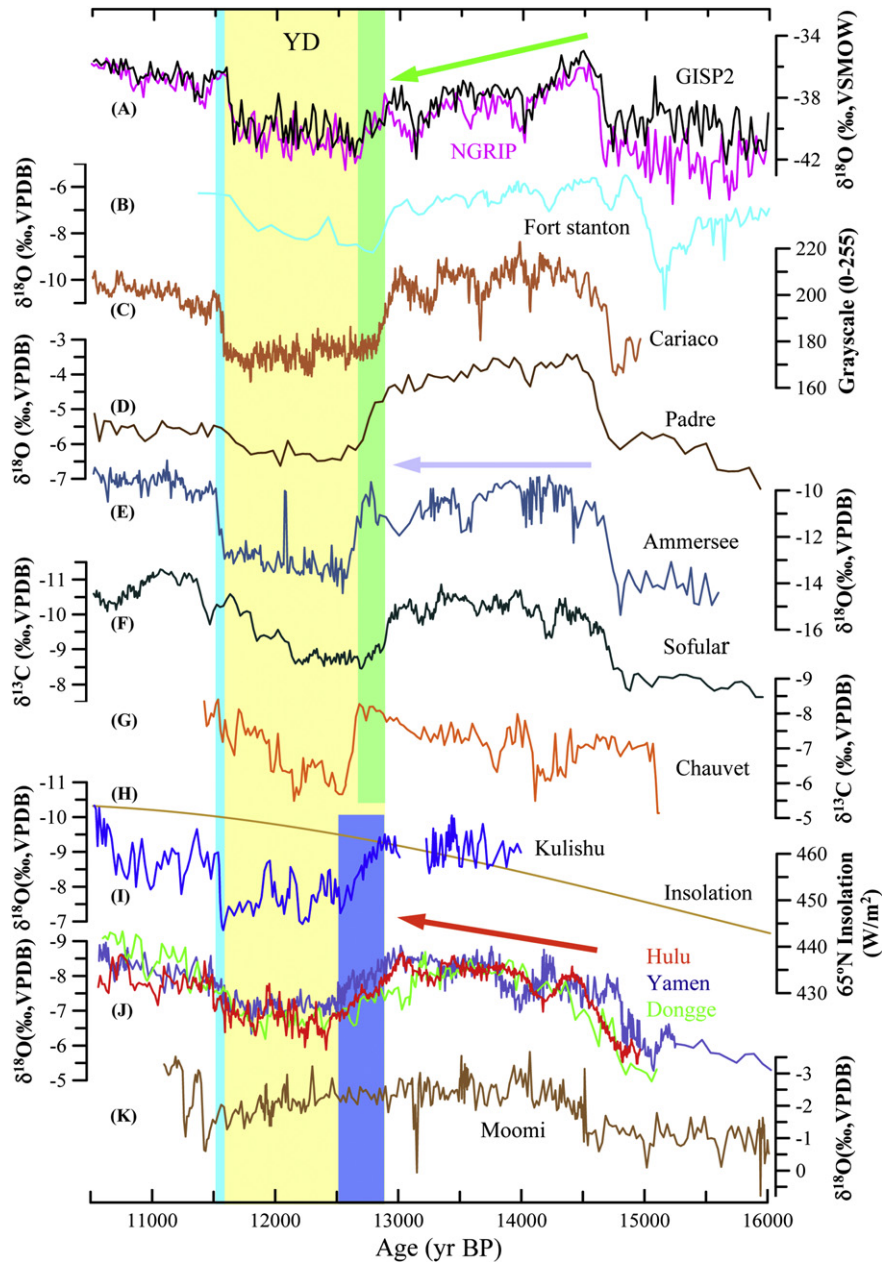
Fig. 7. Comparison of high-resolution climate records between 16 and 10 ka BP from different climate regimes. (A) Greenland ice core records GISP2 (black, Stuiver and Grootes, 2000) and NGRIP (pink, Rasmussen et al., 2006). (B) The Fort Stanton Cave $\delta^{18}O$ record from southwestern USA (Asmerom et al., 2010). (C) The record of sediment grayscale values from the Cariaco basin, Venezuela (Hughen et al., 1996). (D) The Padre Cave $\delta^{18}O$ record from Brazil (Wang et al., 2007). (E) The Lake Ammersee $\delta^{18}O$ record from Germany (von Grafenstein et al., 1999). (F) The Sofular Cave $\delta^{13}C$ record from Turkey (Fleitmann et al., 2009). (G) The Chauvet $\delta^{13}C$ record from France (Genty et al., 2006). (H) Summer (June–August) insolation at 65°N (Berger, 1978). (I) The Kulishu Cave $\delta^{18}O$ record. (J) Three Chinese $\delta^{18}O$ records from Hulu (red, Wang et al., 2001), Dongge (green, Dykoski et al., 2005) and Yamen (blue, Yang et al., 2010) Caves. (K) The Moomi Cave $\delta^{18}O$ record from Yemen (Shakun et al., 2007). The light-blue bar indicates the relatively abrupt termination of the YD event. The green and dark blue bars show the relatively rapid and more gradual transitions into the YD event around the Atlantic Ocean and in AM regions, respectively. Three arrows illustrate different Bølling-Allerød trends among Atlantic sector rising trend (records (A), (C) and (D)), the Germany/Turkey flat trend (records (E) and (F)), and the AM-type trend (records (G) and (I)–(K)). Record locations are shown in Fig. 8. (For interpretation of the references to color in this figure legend, the reader is referred to the web version of this article.)

5.2. North Atlantic forcing and millennial-scale variability

While AM variability broadly follows insolation on orbital-scales, it is also punctuated by numerous millennial and centennial scale events, including the YD (Wang et al., 2008; Cheng et al., 2009b). Therefore, the AM responds to orbital forcing and likely anomalies in North Atlantic climate. The latter may be responsible for much of the variability in the AM on millennial and centennial scales. The structure of the YD event in the AM region is similar to millennial-scale events during the last glacial portion of the records, and is consistent with a North Atlantic origin for the event (Alley, 2000).

Recent speleothem records from South America (Wang et al., 2007) showed that the YD was a strong South American Summer Monsoon (SASM) event, anti-phased with its AM counterpart in Northern Hemisphere (Figs. 7 and 8), further demonstrating the global extent of the YD event. The anti-phased relationship between the AM and SASM during the YD event may be tied to
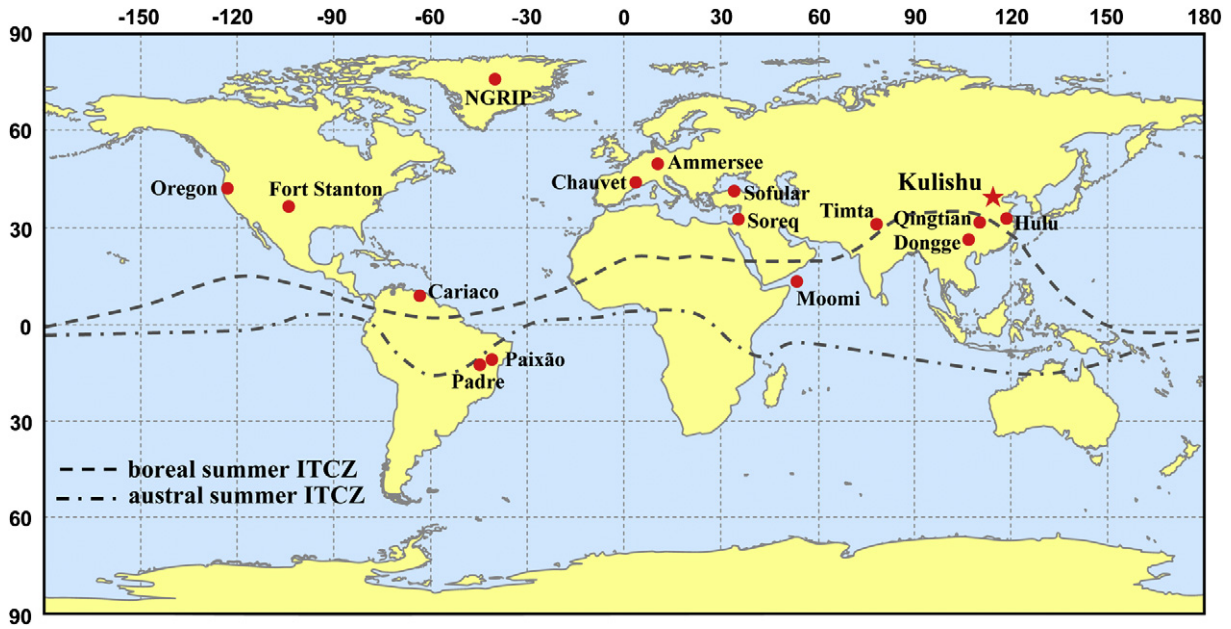
Fig. 8. Location map of the various climate records discussed in the text and Fig. 7. The dashed lines mark modern positions of the ITCZ during summer and winter (adapted from Shakun et al., 2007).

changes in Atlantic Meridional Overturning Circulation (AMOC), which affect North Atlantic climate and in turn affect the monsoon and the mean latitudinal position of the Intertropical Convergence Zone (ITCZ), resulting in the observed low-latitude precipitation patterns (e.g., Wang et al., 2004, 2007). The link between North Atlantic climate forcing and AM variability has been well established (Wang et al., 2001), and the teleconnection between the Greenland and Chinese stadial–interstadials is also convincing (Cheng et al., 2006, 2009b; Wang et al., 2008; Ziegler et al., 2010). Climate simulations support such a link as well (Mikolajewicz et al.,

Fig. 9. Comparison of Greenland ice core NGRIP (A) (Rasmussen et al., 2006) with the Kulishu record (B). Three yellow bars indicate three possible warm events in NGRIP record (A1−A3) that possibly correlate to three events in the Kulishu record (A1′−A3′). The gray bar indicates the abrupt termination of the YD event. Note that the NGRIP timescale is shifted to young ages by 80 yrs (within combined age errors of both records). (For interpretation of the references to color in this figure legend, the reader is referred to the web version of this article.)

1997; Chiang and Bitz, 2005; Zhang and Delworth, 2005). Further simulations and additional high-resolution geological records representing different climate systems are critical to provide further tests of the AMOC hypothesis, but at this time it appears to be the most plausible explanation for the above observations.

5.3. Insolation forcing

On orbital timescales, it is also clear that AM/SASM changes broadly follow Northern/Southern Hemisphere summer insolation (Cruz et al., 2005; Wang et al., 2007, 2008; Cheng et al., 2009b). This observation is consistent with the idea originally proposed by Kutzbach (see Kutzbach et al., 2008 and references therein) regarding insolation forcing in the context of orbital-scale changes.

AM researchers were once puzzled by the increase in AM intensity during the Bølling-Allerød period, inferred from the Hulu $\delta^{18}O$ excursion (Wang et al., 2001), in the context of generally decreasing Greenland temperature over this interval (Fig. 7). While all AM records show an increasing trend similar to the Hulu record during the Bølling-Allerød period, some records from the Atlantic region do not. The Cariaco Basin record (Hughen et al., 1996) displays a decreasing trend, similar to Greenland temperature records and opposite to its South American counterpart the SASM record (Fig. 7). It is likely that the gradual and small temperature decrease observed in the North Atlantic region may have had a relatively limited impact on the AM system, or does not supersede the affect of orbital forcing at this time of rapidly rising of Northern Hemisphere summer insolation. We propose that the increasing AM trend is driven dominantly by insolation forcing, in contrast to the climate of the North Atlantic basin (Fig. 7). However, in Western Europe, the $\delta^{18}O$ record from Lake Ammersee (von Grafenstein et al., 1999) shows a rather flat Bølling-Allerød period, whereas the Chauvet Cave $\delta^{13}C$ record (Genty et al., 2006) shows an increasing trend (interpreted as a progressive increase in temperature) during the Bølling-Allerød period, similar to the AM records. The authors suggest that the Chauvet $\delta^{13}C$ trend can also be attributed to insolation forcing which possibly superseded North Atlantic forcing during the Bølling-Allerød period (Genty et al., 2006).
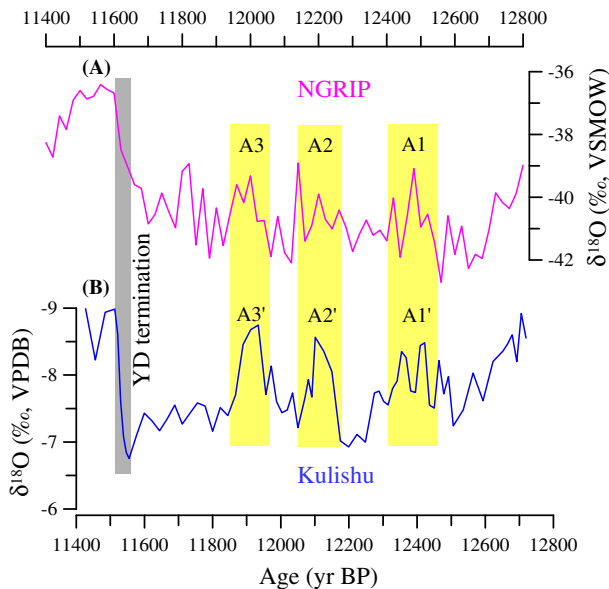
5.4. Interplay between insolation and North Atlantic forcings

Insolation may well have played a role in the differences observed between the YD and Heinrich Stadial 1 (HS1) events in the AM records. The YD and HS1 are both weak monsoonal events that likely originated in the North Atlantic, but during the YD, the AM did not reach the extremely heavy $\delta^{18}O$ values that are observed during HS1. Average values during the weak AM event were approximately 1.3‰ heavier during HS1 than during the YD in the Hulu Cave record, and similar differences are observed in other Chinese cave records (Dykoski et al., 2005; Wang et al., 2008; Yang et al., 2010). One aspect of climate that could account for the disparity in $\delta^{18}O$ values is that Northern Hemisphere summer insolation was at a relative low during HS1, while during the YD event, insolation was approaching its peak. Furthermore, the amplitude of the AM YD event is relatively small compared to the associated temperature change in Greenland, which shifted from near-interglacial conditions back to values similar to those prior to Termination I (Fig. 7). Again, this pattern may demonstrate the strong influence of insolation forcing on the AM.

6. Conclusions

The speleothem $\delta^{18}O$ record from Kulishu Cave reconstructs a high-resolution and absolute-dated AM history between ∼ 14 and 10.5 ka BP in northern China. Consistent with previously reported AM records from central and southern China, the YD event in the Kulishu record behaves as a weak monsoon period between 12,850 ± 40 and 11,510 ± 40 yr BP with an asymmetrical structure characterized by a gradual transition into the YD (340 yrs) and an abrupt ending (20 yrs). The detailed, asymmetric AM YD structure is consistent across China. However, records from Greenland and around the North Atlantic basin may have experienced a more abrupt transition into the YD. Insolation plays a major role in shaping the AM climate on orbital timescales, but also influences the structure of millennial-scale events long enough in duration for insolation to have changed significantly. The combined effect of North Atlantic anomalies and insolation changes is likely responsible for the opposing trends of the AM and Greenland temperature during the Bølling-Allerød period and the difference in Greenland temperature shift and AM shift between HS1 and the YD.

References

Alley, R.B., 2000. The Younger Dryas cold interval as viewed from central Greenland. Quaternary Science Reviews 19, 213–226.
Alley, R.B., Meese, D.A., Shuman, C.A., Gow, A.J., Taylor, K.C., Grootes, P.M., White, J.W.C., Ram, M., Waddington, E.D., Mayewski, P.A., Zielinski, G.A., 1993. Abrupt increase in Greenland snow accumulation at the end of the Younger Dryas event. Nature 362, 527–529.
Asmerom, Y., Polyak, V.J., Burns, S.J., 2010. Variable winter moisture in the southwestern United States linked to rapid glacial climate shifts. Nature Geoscience 3, 114–117.

Bar-Matthews, M., Ayalon, A., Gilmour, M., Matthews, A., Hawkesworth, C.J., 2003. Sea–land oxygen isotopic relationships from planktonic foraminifera and speleothems in the Eastern Mediterranean region and their implication for paleorainfall during interglacial intervals. Geochimica et Cosmochimica Acta 67, 3181–3199.
Berger, A.L., 1978. Long-term variations of caloric insolation resulting from the Earth's orbital elements. Quaternary Research 9, 139–167.
Broecker, W.S., Denton, G.H., Edwards, R.L., Cheng, H., Alley, R.B., Putnam, A.E., 2010. Putting the Younger Dryas cold event into context. Quaternary Science Reviews 29, 1078–1081.
Cai, B.G., Edwards, R.L., Cheng, H., Tan, M., Wang, X., Liu, T.S., 2008. A dry episode during the Younger Dryas and centennial-scale weak monsoon events during the early Holocene: a high-resolution stalagmite record from southeast of the Loess Plateau, China. Geophysical Research Letters 35, L02705. doi:10.1029/2007GL030986.
Cheng, H., Edwards, R.L., Hoff, J., Gallup, C.D., Richards, D.A., Asmerom, Y., 2000. The half-lives of uranium-234 and thorium-230. Chemical Geology 169, 17–33.
Cheng, H., Edwards, R.L., Wang, Y.J., Kong, X.G., Ming, Y.F., Kelly, M.J., Wang, X.F., Gallup, C.D., Liu, W.G., 2006. A penultimate glacial monsoon record from Hulu Cave and two-phase glacial terminations. Geology 34, 217–220.
Cheng, H., Fleitmann, D., Edwards, R.L., Wang, X.F., Cruz, F.W., Auler, A.S., Mangini, A., Wang, Y.J., Kong, X.G., Burns, S.J., Matter, A., 2009a. Timing and structure of the 8.2 kyr B.P. event inferred from $\delta^{18}O$ records of stalagmites from China, Oman, and Brazil. Geology 37, 1007–1010.
Cheng, H., Edwards, R.L., Broecker, W.S., Denton, G.H., Kong, X.G., Wang, Y.J., Zhang, R., Wang, X.F., 2009b. Ice age terminations. Science 326, 248–252.
Chiang, J.C.H., Bitz, C.M., 2005. Influence of high latitude ice cover on the marine Intertropical Convergence Zone. Climate Dynamics 25, 477–496.
Cruz, F.W., Burns, S.J., Karmann, I., Sharp, W.D., Vuille, M., Cardoso, A.O., Ferrari, J.A., Dias, P.L.S., Viana Jr., O., 2005. Insolation-driven changes in atmospheric circulation over the past 116,000 years in subtropical Brazil. Nature 434, 63–66.
Cruz, F.W., Vuille, M., Burns, S.J., Wang, X.F., Cheng, H., Werner, M., Edwards, R.L., Karmann, I., Auler, A.S., Nguyen, H., 2009. Orbitally driven east-west antiphasing of South American precipitation. Nature Geoscience 2, 210–214.
Dansgaard, W., 1964. Stable isotopes in precipitation. Tellus 16, 436–468.
Dykoski, C.A., Edwards, R.L., Cheng, H., Yuan, D.X., Cai, Y.J., Zhang, M.L., Lin, Y.S., Qing, J.M., An, Z.S., Revenaugh, J., 2005. A high-resolution, absolute-dated Holocene and deglacial Asian monsoon record from Dongge Cave, China. Earth and Planetary Science Letters 233, 71–86.
Edwards, R.L., Chen, J.H., Wasserburg, G.J., 1987. $^{238}U-^{234}U-^{230}Th-^{232}Th$ systematic and the precise measurement of time over the past 500,000 years. Earth and Planetary Science Letters 81, 175–192.
Fleitmann, D., Cheng, H., Badertscher, S., Edwards, R.L., Mudelsee, M., Göktürk, O.M., Fankhauser, A., Pickering, R., Raible, C., Matter, A., Kramers, J., Tüysüz, O., 2009. Timing and climatic imprint of Dansgaard-Oeschger events in stalagmites from Northern Turkey. Geophysical Research Letters 36, L19707. doi:10.1029/2009GL040050.
Genty, D., Blamart, D., Ghaleb, B., Plagnes, V., Causse, Ch., Bakalowicz, M., Zouari, K., Chkir, N., Hellstrom, J., Wainer, K., Bourges, F., 2006. Timing and dynamics of the last deglaciation from European and North African $\delta^{13}C$ stalagmite profiles—comparison with Chinese and South Hemisphere stalagmites. Quaternary Science Reviews 25, 2118–2142.
Griffiths, M.L., Drysdale, R.N., Gagan, M.K., Zhao, J.X., Ayliffe, L.K., Hellstrom, J.C., Hantoro, W.S., Frisia, S., Feng, Y.X., Cartwright, I., St. Pierre, E., Fischer, M.J., Suwargadi, B.W., 2009. Increasing Australian–Indonesian monsoon rainfall linked to early Holocene sea-level rise. Nature Geoscience 2, 636–639.
Haug, G.H., Hughen, K.A., Sigman, D.M., Peterson, L.C., Rohl, U., 2001. Southward migration of the intertropical convergence zone through the Holocene. Science 293, 1304–1308.
Hendy, C.H., 1971. The isotopic geochemistry of speleothem—I. The calculation of the effects of different models of formation on the isotopic composition of speleothems and their applicability as palaeoclimatic indicators. Geochimica et Cosmochimica Acta 35, 801–824.
Hughen, K.A., Overpeck, J.T., Peterson, L.C., Trumbore, S., 1996. Rapid climate changes in the tropical Atlantic region during the last deglaciation. Nature 380, 51–54.
Kelly, M.J., Edwards, R.L., Cheng, H., Yuan, D.X., Cai, Y., Zhang, M.L., Lin, Y.S., An, Z.S., 2006. High resolution characterization of the Asian Monsoon between 146,000 and 99,000 years B.P. from Dongge Cave, China. Paleogeography, Paleoclimatology, Paleoecology 236, 20–38.
Ku, T.L., Li, H.C., 1998. Speleothems as high-resolution paleoenvironment archives: records from northeastern China. Proceedings of the Indian Academy of Sciences (Earth and Planetary Sciences) 107, 321–330.
Kutzbach, J.E., Liu, X.D., Liu, Z.Y., Chen, G.S., 2008. Simulation of the evolutionary response of global summer monsoons to orbital forcing over the last 280,000 years. Climate Dynamics 30, 567–579.
Lachniet, M.S., 2009. Climatic and environmental controls on speleothem oxygen-isotope values. Quaternary Science Reviews 28, 412–432.
Li, H.C., Ku, T.L., Yuan, D.X., Wan, N.J., Ma, Z.B., Zhang, P.Z., Bar-Matthews, M., Ayalon, A., Liu, Z.H., Zhang, M.L., Zhu, Z.Y., Wang, R.M., 2007. Stable isotopic compositions of waters in the karst environments of China: climatic implications. Applied Geochemistry 22, 1748–1763.
Liu, D.B., Wang, Y.J., Cheng, H., Edwards, R.L., Kong, X.G., Wang, X.F., Wu, J.Y., Chen, S.T., 2008. A detailed comparison of Asian monsoon intensity and

Greenland temperature during the Allerod and Younger Dryas events. Earth and Planetary Science Letters 272, 691–697.

Meese, D.A., Gow, A.J., Alley, R.B., Zielinski, G.A., Grootes, P.M., Ram, M., Taylor, K.C., Mayeski, P.A., Bolzan, J.F., 1997. The Greenland Ice Sheet Project 2 depth-age scale: methods and results. Journal of Geophysical Research 102, 26411–26423.

Mikolajewicz, U., Crowley, T.J., Schiller, A., Voss, R., 1997. Modeling teleconnections between the North Atlantic and North Pacific during the Younger Dryas. Nature 387, 384–387.

Peng, Y.J., Xiao, J.L., Nakamura, T., Liu, B., Inouchi, Y., 2005. Holocene East Asian monsoonal precipitation pattern revealed by grain-size distribution of core sediments of Daihai Lake in Inner Mongolia of north-central China. Earth and Planetary Science Letters 233, 467–479.

Rasmussen, S.O., Andersen, K.K., Svensson, A.M., Steffensen, J.P., Vinther, B.M., Clausen, H.B., Siggaard-Andersen, M.-L., Johnsen, S.J., Larsen, L.B., Dahl-Jensen, D., Bigler, M., Röthlisberger, R., Fischer, H., Goto-Azuma, K., Hansson, M.E., Ruth, U., 2006. A new Greenland ice core chronology for the last glacial termination. Journal Geophysical Research 111, DO6102.

Severinghaus, J.P., Sowers, T., Brook, E.J., Alley, R.B., Bender, M., 1998. Timing of abrupt climate change at the end of the Younger Dryas interval from thermally fractionated gases in polar ice. Nature 391, 141–146.

Shakun, J.D., Burns, S.J., Fleitmann, D., Kramers, J., Matter, A., Ai-Subary, A., 2007. A high-resolution, absolute-dated deglacial speleothem record of Indian Ocean climate from Socotra Island, Yemen. Earth and Planetary Science Letters 259, 442–456.

Shen, C.C., Edwards, R.L., Cheng, H., Dorale, J.A., Thomas, R.B., Bradley Moran, S., Weinstein, S.E., Edmonds, H.N., 2002. Uranium and thorium isotopic and concentration measurements by magnetic sector inductively coupled plasma mass spectrometry. Chemical Geology 185, 165–178.

Sinha, A., Cannariato, K.G., Stott, L.D., Li, H.C., You, C.F., Cheng, H., Edwards, R.L., Singh, I.B., 2005. Variability of southwest Indian summer monsoon precipitation during the Bølling-Allerød. Geology 33, 813–816.

Stuiver, M., Grootes, P.M., 2000. GISP2 oxygen isotope ratios. Quaternary Research 53, 277–284.

Sun, X., Chen, Y., 1991. Palynological records of the last 11,000 years in China. Quaternary Science Reviews 10, 537–544.

Tan, M., Liu, D.S., Hou, J.Z., Qin, X.G., Zhang, H.C., Li, T.Y., 2003. Cyclic rapid warming on centennial-scale revealed by a 2650-year stalagmite record of warm season temperature. Geophysical Research Letters 30, 191–194.

Tan, M., Baker, A., Genty, D., Smith, C., Esper, J., Cai, B.G., 2006. Applications of stalagmite laminae to paleoclimate reconstructions: comparison with dendro-chronology/climatology. Quaternary Science Reviews 25, 2103–2117.

Vacco, D.A., Clark, P.U., Mix, A.C., Cheng, H., Edwards, R.L., 2005. A speleothem record of Younger Dryas cooling from the Klamath Mountains, Oregon. Quaternary Research 64, 249–256.

von Grafenstein, U., Erlenkeuser, H., Braauer, A., Jouzel, J., Johnsen, S.J., 1999. A mid-European decadal isotope-climate record from 15,500 to 5000 years B.P. Science 284, 1654–1657.

Wang, S.M., Ji, L., Yang, X.D., Xue, B., Ma, Y., Hu, S.Y., 1994. The record of Younger Dryas event in Lake sediments from Jalai Nur, Inner Mongolia. Chinese Science Bulletin 39, 831–835.

Wang, X.F., Auler, A.S., Edwards, R.L., Cheng, H., Cristalli, P.S., Smart, P.L., David, A., Richards, D.A., Shen, C.C., 2004. Northeastern Brazil wet periods linked to distant climate anomalies and rainforest boundary changes. Nature 432, 740–743.

Wang, X.F., Edwards, R.L., Auler, A.S., Cheng, H., Ito, E., 2007. Millennial-scale interhemispheric asymmetry of low-latitude precipitation: speleothem evidence and possible high-latitude forcing. In: Schmittner, A., et al. (Eds.), Ocean Circulation: Mechanisms and Impacts. Past and Future Changes of Meridional Overturning: American Geophysical Union Geophysical Monograph 173, pp. 279–294.

Wang, Y.J., Cheng, H., Edwards, R.L., An, Z.S., Wu, J.Y., Shen, C.C., Dorale, J.A., 2001. A high-resolution absolute-dated late Pleistocene monsoon record from Hulu Cave, China. Science 294, 2345–2348.

Wang, Y.J., Cheng, H., Edwards, R.L., Kong, X.G., Shao, X., Chen, S.T., Wu, J.Y., Jiang, X., Wang, X.F., An, Z.S., 2008. Millennial-and orbital-scale changes in the East Asian monsoon over the past 224,000 years. Nature 451, 1090–1093.

Wei, L.Y., Peng, G., Yan, F.H., Yin, J.H., Lu, Y.C., Liu, R.M., 1997. Climatic changes and their environmental effects during the last deglaciation in Beijing area. Quaternary Sciences (in Chinese) 2, 183–191.

Yang, Y., Yuan, D.X., Cheng, H., Zhang, M.L., Qin, J.M., Lin, Y.S., Zhu, X.Y., Edwards, R.L., 2010. Precise dating of abrupt shifts in the Asian Monsoon during the last deglaciation based on stalagmite data from Yamen Cave, Guizhou Province, China. Science in China Series D Earth Sciences 53 (5), 633–641.

Yi, S., Saito, Y., 2004. Latest Pleistocene climate variation of the East Asian monsoon from pollen records of two East China regions. Quaternary International 121, 75–87.

Yuan, D.X., Cheng, H., Edwards, R.L., Dykoski, C.A., Kelly, M.J., Zhang, M.L., Qin, J.M., Lin, Y.S., Wang, Y.J., Wu, J.Y., Dorale, J.A., An, Z.S., Cai, Y.J., 2004. Timing, duration, and transitions of the last interglacial Asian monsoon. Science 304, 575–578.

Zhang, R., Delworth, T.L., 2005. Simulated tropical response to a substantial weakening of the Atlantic thermohaline circulation. Journal of Climate 18, 1853–1860.

Zhou, W.J., Head, M.J., Deng, L., 2001. Climate changes in northern China since the late Pleistocene and its response to global change. Quaternary International 83–85, 285–292.

Ziegler, M., Tuenter, E., Lourens, L.J., 2010. The precession phase of the boreal summer monsoon as viewed from the eastern Mediterranean (ODP Site 968). Quaternary Science Reviews 29, 1481–1490.